



Inter IIT Tech Meet 13.0

## High-Resolution Elemental Mapping of Lunar Surface

### **ENDTERM REPORT**

SUBMITTED BY:

**TEAM 30**

*The report outlines elemental mapping of the lunar surface using data from Chandrayaan-2's X-ray fluorescence (XRF) spectrometer (CLASS) and details data processing techniques and aims to create high-resolution elemental ratio maps for geochemical analysis.*

## Contents

<b>1. Introduction of Problem Statement</b>	<b>4</b>
<b>2. Literature Review</b>	<b>5</b>
2.A. CLASS Overview . . . . .	5
2.B. XSM Overview . . . . .	5
2.B.I. X-ray Solar Monitor (XSM) . . . . .	5
2.B.II. PHA and GTI . . . . .	6
2.C. Flares and spectrum . . . . .	7
2.D. Geographic Composition . . . . .	7
<b>3. Methodology</b>	<b>8</b>
3.A. Data Retrieval . . . . .	8
3.A.I. CLASS . . . . .	8
3.A.II. XSM . . . . .	9
3.B. CLASS Data Classification . . . . .	9
3.C. Data Preprocessing . . . . .	10
3.C.I. Background Removal . . . . .	11
3.D. Elemental Peak Identification . . . . .	12
3.E. Mapping Coverages . . . . .	14
3.F. Spectral Fitting and Normalization . . . . .	14
3.G. Calculating Ratios and finding compositional groups . . . . .	15
3.H. Determining Best Ratios . . . . .	16
3.I. Sub pixel Resolution . . . . .	16
<b>4. Observations and Results</b>	<b>18</b>
4.A. XRF Catalog . . . . .	18
4.B. Coverage Maps . . . . .	18
4.B.I. Analysis of Coverage Maps : . . . . .	19
4.C. Achieve Subpixel Resolution . . . . .	19
4.D. Elemental ratio maps . . . . .	20
4.D.I. Sub pixel Resolution : . . . . .	21
4.E. Uncertainty Quantification . . . . .	21
4.F. Visualization at finer scale(1.25km × 1.25km) . . . . .	23
<b>5. Flow Chart of Procedure</b>	<b>26</b>
<b>6. Challenges and Lessons Learnt</b>	<b>27</b>
<b>7. Future Scope and Recommendations</b>	<b>27</b>
<b>8. References</b>	<b>28</b>

## List of Figures

1. XSM Flow Chart . . . . .	6
2. Detecting and Extracting Orbits . . . . .	10
3. Geotail Interference . . . . .	11
4. Different components of the observed and calculated spectra . . . . .	13
5. Grids representing 6.25, 3.125, and 1.25 km width respectively . . . . .	18
6. Coverage Maps of Al and Mg . . . . .	18

7.	Coverage Maps of Fe and Ca. . . . .	18
8.	Coverage Maps of Cr and O. . . . .	19
9.	Coverage Maps of Ti and Si . . . . .	19
10.	Comparison of resolution between $12.5\text{km} \times 12.5\text{km}$ and $1.25 \times 1.25\text{km}$ . . . . .	19
11.	Elemental Ratio Maps: Mg/Si and Al/Si Ratios. . . . .	20
12.	Elemental Ratio Maps: Mg/O and Al/O Ratios . . . . .	20
13.	Elemental Ratio Maps:O/Si and Ca/Si Ratio . . . . .	20
14.	Elemental Ratio Maps at 3.125 km resolution: Mg/Si and Al/Si Ratios . . . . .	21
15.	Elemental Ratio Maps at 3.125 km resolution: Mg/O and Al/O Ratios. . . . .	21
16.	Elemental Ratio Map at 3.125 km resolution: O/Si Ratios. . . . .	21
17.	Comparison of Al/Si ratio uncertainty map and box plot. . . . .	22
18.	Comparison of Mg/Si ratio uncertainty map and box plot. . . . .	22
19.	Comparison of O/Si ratio uncertainty map and box plot. . . . .	22
20.	Comparison of Al/O ratio uncertainty map and box plot. . . . .	23
21.	Comparison of Mg/O ratio uncertainty map and box plot. . . . .	23
22.	Elemental Ratio Maps at Mare Fecunditatis . . . . .	23
23.	Elemental Ratio Maps at Mare Vaporum . . . . .	24
24.	Elemental Ratio Maps at Mare Insularum . . . . .	24
25.	Elemental Ratio Maps at Copernicus crater . . . . .	25

## List of Tables

1.	Solar flare classes and characteristics . . . . .	7
2.	Characteristic K-alpha Peak Energy Levels for Various Elements . . . . .	12

## 1. Introduction of Problem Statement

India's Chandrayaan-2 mission, launched on July 22, 2019, aboard the GSLV MK-3 rocket from the Satish Dhawan Space Centre, was a major stepping stone in the field of lunar exploration. Targeting the Moon's South Polar region, which no one had ever reached before, this mission was designed to probe areas of the lunar surface that remain largely uncharted, especially its dark side, aiming to uncover valuable insights into the Moon's surface composition and the potential presence of water.

The mission majorly has 2 objectives:

1. To understand our Moon's history and gain insights into the evolution of the Solar System.
2. To explore the origin and the evolution of our Moon.

**The problem statement aims to generate elemental ratio maps of the lunar surface using the CLASS dataset from the Chandrayaan-2 mission.**

X-ray fluorescence allows for the detection and quantification of lunar compositional elements. When high-energy solar X-rays hit the lunar surface, ejection of electrons from the inner shells of atoms occurs. Once the electron is ejected, other electrons from an outer orbital fill the space almost instantaneously, releasing element-specific energy, in this case, in the form of X-rays (fluorescence photons) that are measured by a detector. The element-specific fluorescence wavelength permits a qualitative determination, while the intensity of the emission provides a quantitative analysis. The characteristic energy depends on the orbital from which the electron is removed and the filling electron orbital. X-ray fluorescence (XRF) lines are detected in CLASS during solar flares. The XRF line energy identifies the element, while the intensity depends on solar flare strength, zenith angle, and composition. By analyzing line ratios, the angular dependence and incident solar flux dependence can be mitigated to some extent.

Global XRF line ratio maps with a spatial resolution of 12.5 km by 12.5 km are intended to be generated from CLASS data, representing a new independent map useful for geochemical and resource mapping. This would improve the current resolution of 12.5 km by 150 km. The objective is to utilize the entire set of XRF spectra measured by CLASS to derive XRF line intensities and create a high-resolution elemental ratio map to identify compositional differences on kilometer scales.

### Steps to Achieve the Objective

#### a. Identify XRF Spectra:

- To detect X-ray fluorescence (XRF) lines in the spectra recorded by CLASS during solar flares.
- To determine the corresponding elements based on the detected XRF line energies.

#### b. Model Spectra for XRF Line Flux:

- By using the CLASS data analysis pipeline to model the XRF spectra.
- To extract line fluxes for each detected element.

#### c. Calculate Elemental Ratios:

- To derive elemental ratios such as Mg/Si, Al/Si, and O/Si from the modeled line fluxes.
- To identify ratios that best represent compositional heterogeneity.

#### d. Project Ratios onto Lunar Base Map:

- Overlay the derived elemental ratio data onto a high-resolution lunar albedo base map.
- To create a visually interpretable representation of the data.

**e. Uncertainty Quantification:**

- To estimate and quantify uncertainties in the derived elemental ratios to ensure data reliability.

**f. Achieve Subpixel Resolution:**

- Leverage overlapping orbital tracks to enhance spatial resolution beyond the 12 km baseline.
- Explore techniques for interpolating data at finer scales.

## 2. Literature Review

### 2.A. CLASS Overview

**Introduction:** CLASS (Chandrayaan-2 Large Soft X-Ray Spectrometer) is a fluorescence spectrometer instrument aboard the Chandrayaan 2 orbiter that uses **X-ray Fluorescence** to map the elemental surface abundances. Solar X-rays ionize the component atoms, which in turn emit XRF photons in the respective characteristic elemental energies, in turn, detected by the CLASS instrument, which will be sweeping a detection area of  $12.5\text{km} \times 12.5\text{km}$  in an 8-second orbital motion. These datasets are processed to give element abundances localized to a particular area.

It consists of sixteen **SCDs (Swept Charge Devices)** with a Copper collimator coated with gold above each SCD, ensuring that the X-rays collected are from a specific area of the lunar surface, enhancing the spatial resolution of the measurements. All of the SCDs give an instantaneous FOV (Field of View) of  $12.5\text{km} \times 12.5\text{km}$ .

Each of the SCD has an active geometric area of  $21.1\text{mm} \times 20.8\text{mm}$ . Passive collimators on top of the SCD block a fraction of this area. In addition, the Al filters and the dead layer on the SCD absorb X-ray photons. The effective area available for the collection of X-ray photons is given by

$$A_{\text{eff}}(E) = A_{\text{geom}} \times 16 \times (1 - F) \times X(E) \times \epsilon(E)$$

where,  $A_{\text{eff}}$  is the effective area of CLASS,  $A_{\text{geom}}$  is the active geometric area of each SCD,  $F$  is the collimator blocking fraction,  $X$  is the X-ray transmission through the Al filter, and  $\epsilon$  is the detection efficiency, both as a function of energy.

**X-Ray Fluorescence(XRF):**

XRF allows for the detection and quantification of lunar compositional elements. When high-energy solar X-rays hit the lunar surface, they knock electrons off the inner shells of atoms. Once the electron is ejected, other electrons from an outer orbital fill the space almost instantaneously. Due to the quantum nature of these interactions (when an electron absorbs or releases energy, it is a fixed amount of energy photon that depends on the atomic element and the transition), the transition to a lower energy state releases element-specific energy, in this case, in the form of **X-rays (fluorescence photon)** that are measured by a detector. The element-specific fluorescence wavelength permits a qualitative determination, while the intensity of the emission provides a quantitative analysis. The intensity of the XRF lines from the Moon primarily depends on the strength of the solar flare, lunar surface composition, and angle of incidence of the solar X-rays.

### 2.B. XSM Overview

#### 2.B.I. X-ray Solar Monitor (XSM)

The XSM carries out spectral measurements of the Sun in soft X-rays with an energy resolution better than 180 eV at 5.9 keV. It has a sensor package that houses the detector, front-end electronics, a filter wheel mechanism; a processing electronics package that houses the FPGA-based data acquisition system, power electronics, and spacecraft interfaces. The instrument is fixed-mounted on the Chandrayaan-2 orbiter such

that the spacecraft structures do not obstruct the instrument's field of view (FOV).

The ground calibration of XSM required 3 steps: **Gain Calibration, Spectral Redistribution, and Ancillary Response.**

### **1) Gain Calibration:-**

It involves using both the in-built Fe-55 and external energy sources for calibration. This ensures the instrument's response is linear in the energy range of 1-15keV. Although the observed gain varied slightly with the temperature and position of the instrument itself, it has been corrected by parameterizing the gain behavior based on these factors, allowing in-flight corrections to maintain accurate energy measurements.

### **2) Spectral Redistribution Function (SRF):-**

It describes how the detector detects the photons of characteristic energy and models using the Gaussian function to describe the various peaks and other details such as the exponential tail. A slight error will be seen in the detected energy of the photon owing to the inherent noise and incomplete background charge transfer.

### **3) Ancillary Response Function (ARF):-**

It determines the detector's effective area, which is influenced by factors such as geometric area, collimator response, and transmission through materials like Beryllium filters.

## **2.B.II. PHA and GTI**

**Pulse Height Analyzer(PHA)** : PHA considers the time-series data for the solar continuum in the form of a 60-second exposure array, which records the data for each channel. Through GTI, we map the necessary PHA integrated data and normalize the element amplitudes by dividing the peak amplitude detected for a particular element with the PHA count of the corresponding channel.

**Good Time Interval(GTI)** :In order to incorporate the effects of the solar continuum on the XRF data provided by CLASS, we need to coordinate the XSM file with the CLASS dataset for enhanced results. In order to achieve the same, we coordinate these files through the GTIs, where if the 'STARTIME' of a CLASS file lies in a GTI, the XSM can be used to normalize the Peak Amplitudes detected through the above process.

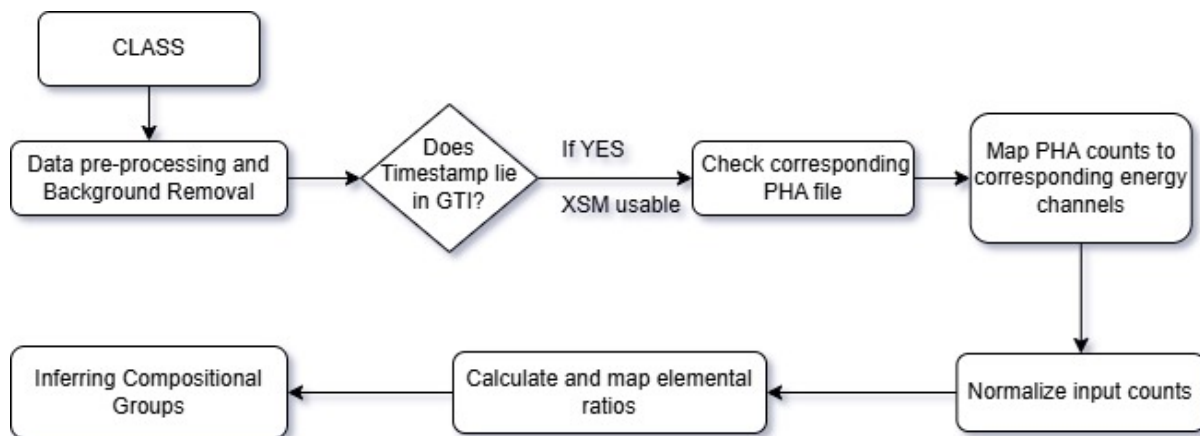


Figure 1: XSM Flow Chart

In case of unavailability of the XSM data, the data from GOES can be used, but it is available as a time-series spectrum of the solar intensity values which makes it cumbersome to convert to usable data as needed. Also owing to the limited availability of the XSM data, in case of its incorporation the coverage gets reduced significantly, due to which it has been discarded.

## 2.C. Flares and spectrum

The excitation of elements occurs when high-energy photons strike the atoms of these elements. Elements have threshold energies required for excitation, allowing electrons to move from one energy level to another. On the lunar surface, this threshold is met when solar flares of significant intensities strike. Solar flare activity is categorized into five classes based on intensity: X, M, C, B, and A as shown in Table 1.

Solar Flare Class	Intensity Range (W/m <sup>2</sup> )	Characteristics
X-Class	$> 10^{-4}$	Strongest flares; enhances signals from elements such as Si, Al, Mg, Fe, Ti, and Ca, even capable of exciting heavy elements like Cr.
M-Class	$10^{-5}$ to $10^{-4}$	Moderate events; can excite Mg, Al, Si, Ca, Fe; less effective at exciting heavier elements.
C-Class	$10^{-6}$ to $10^{-5}$	Mild solar events mainly affect lighter elements like Mg, Al, and Si on the lunar surface.
B-Class	$10^{-7}$ to $10^{-6}$	Low-level activity; primarily excite Mg and Al with higher elements being largely unaffected.
A-Class	$< 10^{-7}$	Very low intensity; generally insufficient to excite detectable fluorescence in any element on the lunar surface.

Table 1: Solar flare classes and characteristics

Since classes X, M, and C provide sufficient excitation for elements such as Mg, Al, Si, Ca, Fe, O, Ti, and Cr, they play a crucial role for achieving the objectives of this study.

## 2.D. Geographic Composition

### Morphology

Three major geological processes influence the formation of the lunar surface: impacts, volcanism, and tectonics. Topography on the moon's near side is divided almost equally between flat basaltic maria and feldspathic highlands, whereas the far side is dominated by highlands crust. Both the near and far sides contain large impact basins, including the South Pole-Aitken Basin, extending from the South Pole up to low southern latitudes on the far side.

### Maria

The lunar maria are the dark, smooth areas on the Moon that are formed when lava flowed across the surface billions of years ago. Geomorphologic features of volcanic origin in lunar maria include (1) lava flows, (2) sinuous rilles, (3) volcanic domes and cones, and (4) pyroclastic deposits. High volumes of low-viscosity, high-temperature basaltic lava erupted in the topographically low-lying impact basin interiors and re-shaped vast areas, i.e., around one-third of the lunar nearside hemisphere is covered by these dark mare deposits.

### Highlands

The lunar highlands are the elevated and light-colored regions on the moon's surface that stand above the dark-colored basins. They feature uneven and irregular surfaces with a large number of craters caused by impacts from space projectiles.

### 3. Methodology

#### 3.A. Data Retrieval

##### 3.A.I. CLASS

Data of X-ray fluorescence (XRF) is captured by the CLASS Instrument of Chandrayaan 2 orbiter. This data contains spectrum files in **FITS(Flexible Image Transport System)** format for an exposure time of 8 seconds in one frame. CLASS raw data is processed at the Payload Operations Centre (POC) into L1 and L2 products for archival at ISSDC. The metadata and the data files contain all necessary information, such as UTC, lunar coordinates, geometry of observation, and file history, necessary for understanding the data set. L1 data is in FITS format. We used Python for Data retrieval and processing.

##### i) Data Downloading:

L1 data during operations (irrespective of XRF signal) is downloaded from PRADAN (<https://pradan.issdc.gov.in/pradan/>).

The downloaded zip file follows a naming convention, for example: cla\_2020Dec10T051032456.zip. Once unzipped, the data directory will be organized as follows: cla/data/calibrated/yyyy/mm/dd/, for instance, cla/data/calibrated/2019/10/29/. Any subsequent data downloads will also unzip into the directory structure cla/data/calibrated/yyyy/mm/dd.

After downloading data from PRADAN, a zip file containing the calibration files, documents, and analysis software should also be downloaded from the 'Other Downloads' page under the 'CLASS' section on the PRADAN website. Once unzipped, the main directory cla contains the following subdirectories: calibration (which holds files required for analysis), document, and miscellaneous.

The '**calibration**' directory contains the files required to carry out analysis:

- 1. class\_rmf\_v1.rmf
- 2. class\_arf\_v1.arf
- 3. background\_all\_events.fits

L1 Combined spectrum for 8 s FITS VIEWER (fv) or ds9: The 'document' directory contains this user manual and SIS document, which provides details of the file naming conventions and formats.

The '**miscellaneous**' directory contains a zip file that provides a software program (CLASS\_add\_L1\_files\_time.pro) written in IDL to add the 8s files. Once the above-mentioned files are downloaded, users can analyze CLASS-calibrated data, as explained in the next sections.

##### ii) Analysis:

The 8-second files are named ch2\_cla\_11\_yyyyymmddTHHMMSS\_yyyyymmddTHHMMSS.fits with the start and end times of the 8 s mentioned in the file name.

```
> fv ch2_cla_11_20200529T104532257_20200529T104540257.fits
```

The 2 x 2048 data has **channel** numbers in the first column and **counts** in the second column.

In CLASS, a photon event is counted and with the energy deposited in the detector, individual X-ray photon interactions in the detector are identified and converted to an electrical signal that is amplified and digitized (the digitized value is termed as '**channel**' hereafter).

### 3.A.II. XSM

The XSM data is archived at the ISRO Science Data Archive (ISDA) hosted at ISSDC. XSM public data can be downloaded from ISDA using the PRADAN web portal at the following link: (<https://pradan.issdc.gov.in/pradan/>)

XSM data is organized as files corresponding to each day of observation (UTC). Zip files with data for any available day of observation can be downloaded from this website. These zip files, having the name of the format ch2\_xsm\_yyyyymmdd\_vx.zip, contain the raw (Level-1) and calibrated (Level-2) data sets of XSM for the given day of observation. When unzipped, this file generates the following directory structure, the root directory being xsm. There will be XML label files associated with each product file, which are not shown here.

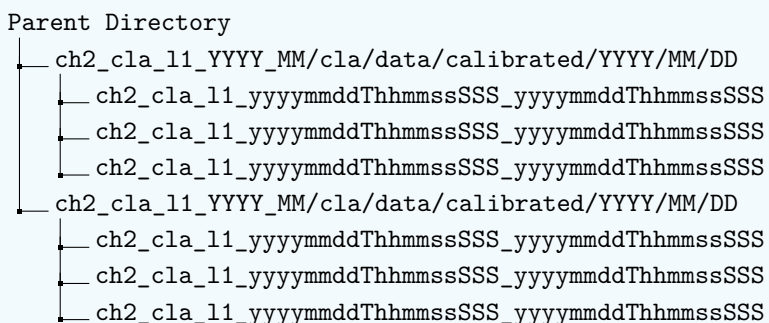
```
xsm/
  data/
    yyyy/
      mm/
        dd/
          raw/
            Ch2_xsm_yyyyymmdd_vx_level1.fits
            Ch2_xsm_yyyyymmdd_vx_level1.hk
            Ch2_xsm_yyyyymmdd_vx_level1.sa
          calibrated/
            Ch2_xsm_yyyyymmdd_vx_level2.gti
            Ch2_xsm_yyyyymmdd_vx_level2.pha
            ch2_xsm_yyyyymmdd_vx_level2.lc
```

This dataset gives us a detailed analysis of solar activity in particular time frames. This dataset can be further used to define the solar continuum and the time of good time intervals around which background can be defined. This will be used further to refine our CLASS data to reach our actual normalized final spectrum to calculate ratios.

### 3.B. CLASS Data Classification

#### Technique for Catalog Generation:-

The data was downloaded in ZIP files from the Pradan Portal. Then, ZIP was unzipped in a common directory. The directory had a final structure:



The Chandrayaan-2 orbiter orbits the moon at an altitude of 100 kilometers (62 miles) with a velocity of 1.56 km/s, thus orbiting a total radius of 1837.4 km (1737.4 km being the lunar radius and 100 km as the orbiter's altitude from the lunar surface) in a total time period of 2.056 hours thus marking the completion of one orbit.

During this orbital motion around the moon, a periodic behavior of the solar angle was observed as it goes from a particular maximum value to a local minima and then back to that maximum value from where it started. The solar angle specifies the angle between the sun's position and the horizontal plane of the lunar surface from the orbiter's position.

The attached figure of Solar Angle vs File Number of a Particular Day shows the periodic behavior of the solar angles as discussed above, while the blue vertical lines signify the peaks and the completion of one orbit too.

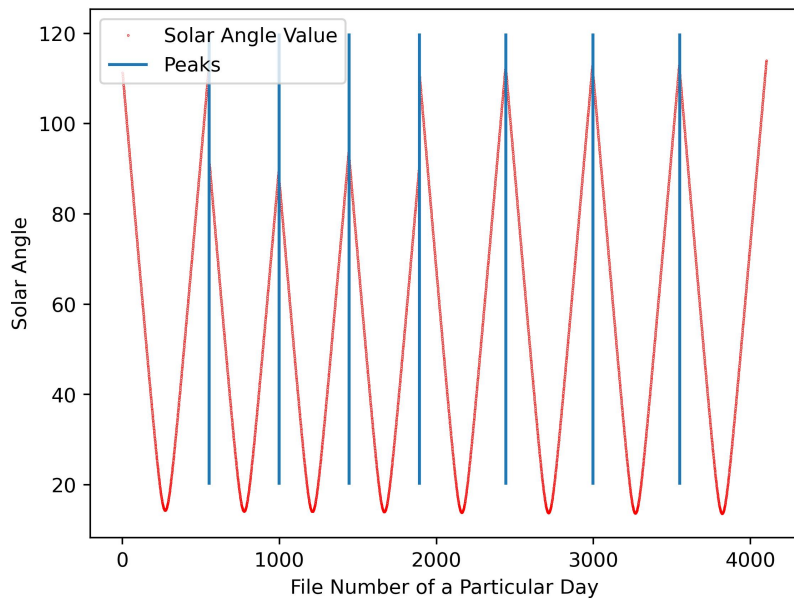


Figure 2: Detecting and Extracting Orbits

After detecting and extracting the orbits, the next task at hand is to segregate the CLASS fits files into night-time and day-time spectrum by incorporating the solar angle concept, the value of which can be taken directly from the CLASS files' 'SOLARANG' header property. The CLASS files having solar angle less than  $90^\circ$  are taken into consideration for day-time spectrum and those having angle larger than  $91^\circ$  are grouped for calculating the background spectrum for that particular orbit. A  $1^\circ$  margin is taken to avoid any effects of the twilight zone in our data.

### 3.C. Data Preprocessing

In X-ray fluorescence (XRF) data analysis, **pre-processing** and **spectral fitting** are crucial steps to obtain meaningful insights from raw observational data. Pre-processing involves cleaning, organizing, and preparing the data for spectral analysis, ensuring that the data is reliable and accurately represents the X-ray emissions from elements present in the target region. For pre-processing, we experimented with two methods: the exponential moving average (EMA) model, a type of moving average that gives more weight to recent observations, making it sensitive to new data points while smoothing out older noise in the dataset. In addition to this, we also experimented with the moving averages (MA) model, which is the primitive version of the one with which we experimented earlier, providing equal weights to all the observations in the corresponding window size.

However, the chosen window size led to the creation of artificial lines at the higher side, thus creating a large coverage (for example, chromium). The moving average technique was thus discarded, for it hampered an optimized smoothening of the CLASS spectra, and the directly find peaks function in Python was used to analyze peaks.

### 3.C.I. Background Removal

The XRF spectra received consist of X-rays emitted due to elemental excitation, Galactic Cosmic Ray (GCR) background, and the scattered solar spectrum. The lunar background in XRF spectra arises from galactic cosmic rays, solar winds, and sporadic bursts of energetic solar particles. These signals mix with genuine elemental emissions, necessitating careful separation for accurate analysis. Lunar background can be clearly seen in night-time observations when there is no interference due to elemental emissions and solar spectrum.

**Geotail Interference:** During the Moon's passage through Earth's geotail, due to XRF emissions from energetic electrons interacting with ions, CLASS observes increased background intensity. This interference, characterized by peaks at aluminum (Al) and iron (Fe), is identified and can be seen in the attached figure below.

- **Night-Time Observations:** Background data is collected when the solar phase angle exceeds  $90^\circ$ , ensuring the Sun does not directly illuminate the lunar surface. During this time, detected X-rays predominantly represent background radiation.
- **Averaging Background Data:** Background data collected during night-time observations is averaged over an orbital pass to account for minor intensity variations caused by the orbiter's position or other external factors. This provides a consistent baseline for analysis.
- **Subtracting Background:** The averaged background data is subtracted from XRF spectra recorded during illuminated phases, isolating true elemental signals from the Galactic Cosmic Ray background. Proper characterization and removal of such background counts are essential for isolating the GCR subtracted lunar elemental emissions.

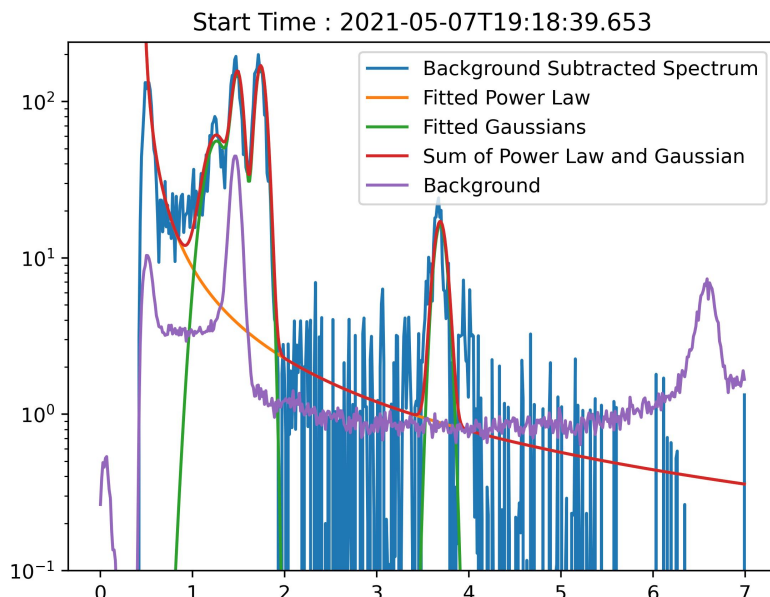


Figure 3: Geotail Interference

### Solar Phase Angle Effects and corresponding Surface Temperature Gradient

The surface temperature gradient on the Moon induces a gradual decrease in spectral peak intensity as the solar phase angle increases. Due to the spherical geometry of the lunar surface, solar spectra illuminate most at the subsolar point, and illumination gradually decreases till the termination zone (solar phase angle  $90^\circ$ ). A

significant gradient in temperature is seen over this range. Post  $90^\circ$ , due to no illumination temperature, the gradient is meager and is negligible around a phase angle of  $180^\circ$ .

To ensure accurate background subtraction, it is required that the background data be consistent with the lunar surface conditions at any given location. Higher solar phase angles provide a more reliable representation of the night-time background.

From our empirical studies, it is observed that:

- The most accurate background data corresponds to solar phase angles near  $180^\circ$ . However, a very limited amount of data is found at this angle.
- A very slight gradient exists near  $90^\circ$ , but the background remains nearly consistent for phase angles between  $90^\circ$  and  $180^\circ$ .

### Threshold Phase Angle for Background Characterization

Due to the limited availability of CLASS data during night-time observations, a threshold solar phase angle of  $91^\circ$  is selected for night-time background characterization. A margin of  $1^\circ$  is necessary to minimize boundary effects. Files corresponding to phase angles  $\geq 91^\circ$  were averaged for each orbital revolution to determine the background counts for that orbit.

### Background Subtraction Process

A systematic process is followed to remove the background, which involves:

1. Identifying and filtering the data files for solar phase angles  $\geq 91^\circ$ .
2. Averaging these filtered files for each orbital revolution to calculate the background counts.
3. Subtracting the background counts from the X-ray fluorescence (XRF) counts on a channel-by-channel basis to generate the final corrected data file.

By following this methodology, the Galactic Cosmic Ray background subtracted CLASS spectrum is finally obtained. [2][3][4]

### 3.D. Elemental Peak Identification

The identification of elemental peaks is crucial for analyzing major lunar surface elements and Chromium (Cr).

Element	K-alpha Peak Energy (keV)
Oxygen (O)	0.525
Magnesium (Mg)	1.25
Aluminum (Al)	1.49
Silicon (Si)	1.74
Calcium (Ca)	3.69
Titanium (Ti)	4.51
Chromium (Cr)	5.41
Iron (Fe)	6.40

Table 2: Characteristic K-alpha Peak Energy Levels for Various Elements

To mitigate fluctuations due to detection errors, we defined a threshold energy range for peak detection.

The energy difference between  $K\alpha$  and  $K\beta$  excitation increases with atomic number, allowing us to safely

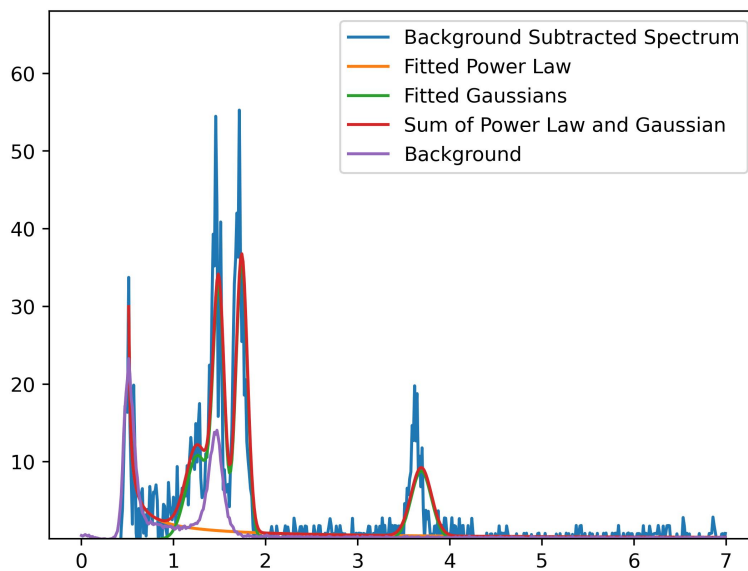


Figure 4: Different components of the observed and calculated spectra

neglect  $K\text{-}\beta$  peaks for elements with higher atomic numbers. For elements with lower atomic numbers, the  $K\text{-}\alpha$  and  $K\text{-}\beta$  peaks are very close to each other. However, due to the lower  $K\text{-}\beta/K\text{-}\alpha$  ratio for lighter elements, we can still safely exclude the  $K\text{-}\beta$  peaks in these elements for our analysis.

The process begins with the identification of the periodic behavior of the solar angle, dropping from a particular maximum value to a local minimum and then back to the same maximum, thus marking the completion of one orbit around the Moon. The orbits were thereby extracted by observing this trend, and the CLASS files were then segregated into daytime (solar angle less than  $90^\circ$ ) and night-time (solar angle greater than  $91^\circ$ ) files for every orbit.

The spectral channels, initially in arbitrary units, are converted into energy units (keV) using a scaling factor of 0.0135. The corresponding counts are then extracted for further analysis. For every orbit, the background data is calculated by averaging the CLASS files' counts from that particular orbit's nighttime files and each daytime file is loaded individually to extract their count values from their respective headers.

To ensure dynamic peak handling, the `find_peaks` function is used with prominence taken as the mean of the `all_counts` (which correspond to the energy channel confined within a range of 0.5keV to 7keV for a refined analysis). This helps to extract the peak indices, which provide the filtered channels and filtered counts where the peaks are identified.

The energy channel closest to the excitation energy of a particular element and the peak amplitude corresponding to that channel are filtered out. For every element, their filtered out peak amplitudes are checked as to whether they lie above the background corresponding to that energy channel. In case of affirmation, the element-wise background (here, taken into account only the Galactic Cosmic Ray background) subtracted peak values, and the energy channel is stored in a CSV file. This includes augmenting the data using its standard deviation ( $3\sigma$  correction) to ensure precision. The values stored for every element serve as the initial guesses for amplitude and center while applying multi-gaussian fitting.

Listing 1: find\_peaks function for determining initial guesses

```
peak_indices = find_peaks(all_counts, prominence=all_counts.mean())
[0]
```

### 3.E. Mapping Coverages

Chandrayaan-2 mission has systematically mapped the lunar surface since September 2019 and continues providing high-quality lunar X-ray spectral data. It has orbited over certain regions of the moon at various times. During its course of exploration, it has covered several regions of the lunar surface and detected XRF data. Elemental presence on the lunar surface over regions is subject to geochemistry and the formation and evolution history of the moon. XRF spectrum recorded peaks for specific elements after spectral processing at a particular geometric coordinate over the lunar surface. For elements, coverage specifies the area over which that particular element was detected. The coverage maps provide significant insights into geochemistry and lunar formation. The elemental coverage of Mg, Al, Si, Ca, Ti, Cr, O, and Fe from five years of CLASS data at a spatial resolution of  $12.5\text{km}(\text{along-track}) \times 12.5\text{km}(\text{across-track})$  are mapped and shown all together in the result section.

The elemental detection data for all elements was stored in a single CSV file with the following structure:

- Latitudes and longitudes of the vertices of the  $12.5\text{km} \times 12.5\text{km}$  spatial resolution acquired from the corresponding file.
- CLASS file Timestamp.
- Element channels and their peak amplitudes (after GCR background subtraction).

### 3.F. Spectral Fitting and Normalization

For every orbit, the occurrence of the start time for the daytime files is checked in the 'Timestamp' column of the CSV file, where the initial guesses are stored before, thus filtering out the corresponding row. For a refined analysis, only the rows where a peak was identified for Mg, Al, and Si are taken into account, and their corresponding amplitude and energy channels for every element in that row are stored. The third parameter for the initial guess, i.e., sigma, is calculated using the concept of Full Width at Half Amplitude (FWHM) and appended into the initial guesses, which stores these three parameters (amplitude, center, and sigma) for every element in case a peak is identified.

The incident solar spectra have different intensities of photons corresponding to different energy values. The excitation of lunar elements is subject to this **solar spectrum**, which causes their excitation. This **solar spectrum** follows behavior similar to a **power law distribution**. The lower intensity of counts in a higher energy range is not necessarily due to a lower abundance of elements corresponding to the excitation energy in that range but is also influenced by a lower number of photons incident at that energy due to the power law distribution behavior of the solar spectra. Similarly, a higher intensity of counts in a lower energy range is not necessarily due to a higher abundance of elements corresponding to excitation energy in that range but also due to a higher number of photons incident at that energy range from the **solar spectrum**.

The obtained counts representing the abundance are relative to the **solar spectrum** causing the excitation. To proceed with obtaining actual relative abundances, the processed, background-removed, and continuum-subtracted spectra are modeled first using **multi-gaussian fit**, where the stored initial guesses for the elements whose peaks were identified are taken into account for fitting the peaks altogether. Next, the Gaussian fitted

peak amplitudes are divided by the **solar continuum** at that period, i.e., corresponding to that element's energy channel. This division yields counts for relative abundances corresponding to a scenario where a unit set of photons is incident for each energy range. This approach provides actual relative abundances, assuming the incident spectrum had an equal number of photons incident across all energy ranges. By doing this, the correct relative abundances of elements present in specific locations are calculated on the lunar surface.

To achieve this, a **power law model** is fitted to the individual CLASS file. This power law model helps accurately model the solar continuum and incorporates the scattered solar spectrum background component.

Listing 2: Power Law model fitting

```
[[a,c,m], err] = curve_fit(powerlaw, (all_channels), (all_counts)
    ,p0 = (np.max(all_counts),0.0,-1.5), maxfev = 155000, bounds
    =((0, -np.inf, -2.5), (4*(np.max(all_counts)), 0 .5, 0 )))
```

This continuum is used to subtract and then divide the processed **XRF spectra**, ensuring an accurate estimation of the relative abundances of lunar elements.

### 3.G. Calculating Ratios and finding compositional groups

The ratios of the elemental abundances relative to Si are calculated as the common criteria. Silicon is chosen as the general standard due to its even distribution over the lunar surface. In the **Apollo 15** and **Apollo 16** experiments, the abundance of **Si** was considered invariant across the lunar surface. Using this assumption, the elemental ratios with respect to Silicon are estimated. This approach requires precise knowledge of the reference element and provides only **relative abundances**. **Si** is used as a general basis for determining elemental ratios, offering insights into the elemental composition of the lunar surface.

**Mg/Si**, **Al/Si**, **Ca/Si**, **Ti/Si**, **Cr/Si**, **O/Si**, **Fe/Si**, **Mg/O**, and **Al/O** ratios were determined. These ratios were calculated with respect to the detected positive peaks of the corresponding elements. Ratios were calculated by dividing the peak intensities of the elements. If either of the elements' signifying peaks was not detected, the ratio could not be calculated. Most of these ratios were found to lie in the range of 0–1. A smaller number of files showed ratio values greater than 1, and for values exceeding 2, few values were quite sparse, which were classified as outliers and thereby filtered out. The calculated ratios were plotted on the **LROC basemap map** based on their location coordinates. Each ratio file was represented as a patch of  $12.5\text{km} \times 12.5\text{km}$ , with a color gradient corresponding to the ratio value.

Studying and understanding the geological significance of the selected ratios is crucial for further analysis. High **Mg/Si** ratios are associated with mare regions on the Moon, particularly in basalts that are rich in magnesium. These regions are darker and volcanic in nature. This is consistent with the composition of the Moon's maria, which contains relatively high amounts of iron and magnesium-rich minerals (e.g., pyroxenes), while on the other hand, the low Mg/Si ratios tend to be found in the highlands, which have a higher concentration of feldspar (an aluminum silicate mineral) and silica-rich rocks. High **Al/Si** ratios indicate the presence of anorthosites in the lunar highlands, which are rich in calcium-aluminum silicates (especially feldspar). These regions are less volcanic and more differentiated in terms of their mineral composition. The regions enriched in silicate-rich volcanic materials, particularly those in the maria, which have a higher concentration of magnesium and iron, point to low Al/Si ratios. High **Ca/Si** ratios are generally found in the highlands, especially in anorthosites, which are calcium-rich feldspar rocks, while low Ca/Si ratios are more common in mare regions with basaltic composition. High **Ti/Si** ratios are found in lunar basalts, especially those rich in ilmenite (a titanium-iron oxide mineral). These high ratios are common in certain mare regions, reflecting regions with significant volcanic activity and differentiation. High **Cr/Si** ratios suggest pyroxene-rich areas, often associated with

volcanic rocks. Pyroxenes, which contain chromium, are indicative of the composition of the lunar mantle and volcanic processes. **O/Si** ratios are used to understand the overall silicate composition of lunar materials. Silicon is a major component of most lunar rocks, and variations in this ratio help differentiate between regions with different silicate compositions, especially in terms of volcanic versus highland compositions. High **Fe/Si** ratios are indicative of iron-rich volcanic rocks such as basalts in the mare regions. This ratio helps identify regions with a significant presence of iron-bearing minerals, often associated with volcanic processes on the Moon. High **Mg/O** ratios are characteristic of regions with basalts (e.g., the mare regions). These areas are enriched in magnesium and iron-bearing minerals, indicating volcanic activity. Such ratios are a sign of areas with significant volcanic history. Areas with high concentrations of feldspar and other aluminum-rich minerals suggest high **Al/O**. These areas are primarily found in the lunar highlands and are key to understanding the early differentiation of the lunar crust.

### 3.H. Determining Best Ratios

Lunar crustal terrain is divided into various geological features. Studies from the Lunar Prospector gamma-ray mission (1998-1999) suggest that the lunar crust and underlying mantle have been divided into distinct terranes that possess unique geochemical, geophysical, and geological characteristics. Lunar geomorphology contains basaltic maria, feldspathic Highland, and impact basins. Each feature contains unique morphology and distinct chemical characteristics. These can be studied through elemental composition maps. Major features, including Mara, Highland, and The South Pole impact basin, were analyzed depending on major elemental ratios with respect to Si, and features showed distinct characteristics.

- The significance of a ratio for analysis depends on various factors such as coverage, uncertainty in ratio values at particular locations during different observations, which defines the reliability of ratios, and heterogeneity in ratio maps, which show compositional variation in different lunar structures.
- The ratios with higher coverage allowed to conduct analysis even in smaller regions. Ratios of lighter or abundant elements with respect to **Si** provide higher coverage due to significant excitation for **XRF**.
- The uncertainty using the **Standard Error of Mean** is calculated; the lower the uncertainty, the higher the reliability of the ratios.

$$\text{SEM}(\text{Mg/Si})(\%) = \frac{\text{Standard Deviation} \cdot 100}{\sqrt{\text{Count}} \cdot \text{Mean}}$$

- Ratios showing variation across different lunar structures helped draw insights about the chemical composition and morphology of those structures. Ratios varying independently of geological structures are of less significance for analysis but could potentially open new areas of research regarding their variation.
- Considering all these factors, **Mg/Si** and **Al/Si** serve as the best ratios for global analysis due to their significant abundance, lower uncertainty, and geological variation.
- Also, elements with globally lower abundance are concentrated in certain lunar structures. For in-situ analysis, these elemental ratios can also serve as the best ratios.

### 3.I. Sub pixel Resolution

**Overlapping Tracks:** Overlapped tracks are used to achieve subpixel resolution. Due to multiple tracks covering the same region, many overlaps are obtained among the tracks. This means that in a  $12.5\text{km} \times 12.5\text{km}$  patch, there are smaller overlapped regions, thus representing data on a finer scale. These overlapped regions can thus be leveraged to get respective intensities by averaging out all the intensities due to multiple overlaps. This is how more detailed information for regions smaller than a  $12.5\text{km} \times 12.5\text{km}$  patch is obtained, making it possible to resolve the initial size of  $12.5\text{km} \times 12.5\text{km}$  into further scales.

Approach : The overlap between two tracks can be viewed as considering 3 different regions where one region that is extra added corresponds to the intersection of both the tracks being overlapped, and its value would include the average out of both the initial values. This averaging out was done taking the best case scenario where there would be 50% overlap. In the case of the original resolution, these smaller regions cannot be recognized with some distinct values.

Improving the resolution 4 times means dividing the initial grid cell of  $12.5\text{km} \times 12.5\text{km}$  into 4 equal sub-parts of  $3.125\text{km} \times 3.125\text{km}$  each. As of now, the grid is divided into 4 sub-grids, and different values can be applied to each of these sub-grids. These smaller regions(overlapped regions) can now be assigned some unique value in the grid. The more grid size is decreased, the more finer the grid is obtained, and the overlapping tracks are better fitted in the grid. This method can give infinite resolution only when the overlapping tracks are dense enough that a reliable value can be obtained at each point.

Sub-pixel resolution is achieved by the methodology given in the steps below:

- **1) Making the Grid:-**

Firstly, a grid is made for mapping the data. Initially, the grid cell size may be taken as  $3.125\text{km} \times 3.125\text{km}$  (can be varied as per requirements). Each grid cell will represent an equal area. Thus, as we go towards the pole, the grid cell size varies. The grid is defined using latitude and longitude bins, which divide the surface into rows and columns. In accordance with the moon's spherical geometry, the distance between two latitude bins always remains the same, and the longitude bin size is the same for the same latitude but decreases as we go towards the poles, i.e. it varies with latitudes. On the Moon, the distance covered per degree latitude is 30.25 km (approximately). It is used to get the latitudinal bin size by dividing our desired distance by this value, thus obtaining the latitudinal bin size. For the Moon, the distance covered per degree of latitude is approximately 30.25 km. Using this, the latitudinal bin size is calculated by dividing our desired distance by this value. The formula for converting a distance in kilometers to longitudinal degrees at a specific latitude is given by :

$$\text{Distance per degree of longitude} = \frac{2\pi R}{360} \cdot \cos(\text{latitude}),$$

where  $R$  is the Moon's radius, and  $\cos(\text{latitude})$  accounts for the reduction in longitudinal distance with increasing latitude.

Through this, the longitudinal and latitudinal bin sizes are obtained, eventually forming the grid by making an array of longitudinal bins for every two consecutive latitudinal bins. This method ensures that the grid cells represent equal areas across the spherical surface.

- **2) Assigning values to the grid:-**

Iterating over each pixel sized  $12.5\text{km} \times 12.5\text{km}$  whose 4 vertices have been given in the form of latitudes and longitudes. Here, a binary search algorithm is used to find the range of grid cells that would contain this pixel. Thus, the ratio value is assigned to each grid cell in this range. After iterating over all the rows, the grid cells that encounter 2 or more assigned intensities, the algorithm averages all the intensities and replaces the value of the grid cell with the average value, taking overlaps into account.

- **3) Plotting the Data:-**

The map is plotted, where each grid cell is colored with respect to these average intensities on the base map of the moon obtained from the LROC website.

As can be seen above, the grid cells, though representing the same area, have increased width when near poles. This methodology ensures that intensity values are obtained for regions smaller than  $12.5\text{km} \times 12.5\text{km}$ .

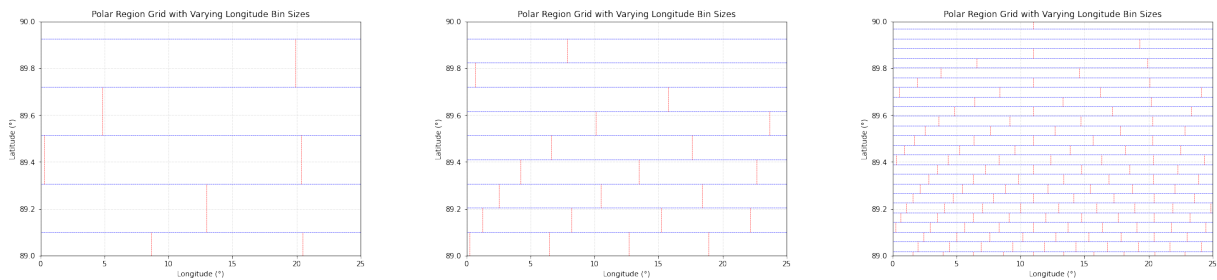


Figure 5: Grids representing 6.25, 3.125, and 1.25 km width respectively

## 4. Observations and Results

### 4.A. XRF Catalog

We obtained the catalog of elemental line detections with their peak intensities for each flare class. A total of 1110 XRF lines were detected in the X class where all the major elements (Mg, Al, and Si) were present. The numbers are 15497, 67209, 12471, and 7 for the M, C, B, and A classes respectively.

### 4.B. Coverage Maps

We obtained the coverage maps of the elements where there were positive intensities in our XRF catalog.

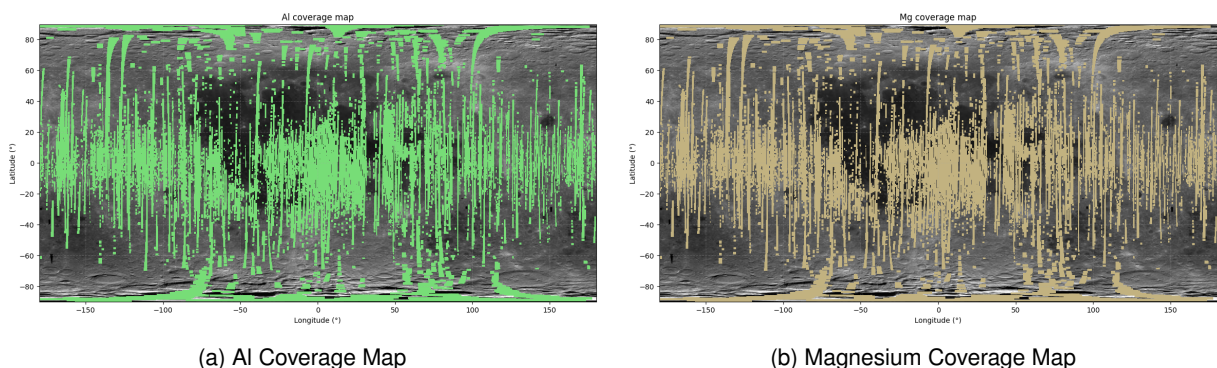


Figure 6: Coverage Maps of Al and Mg.

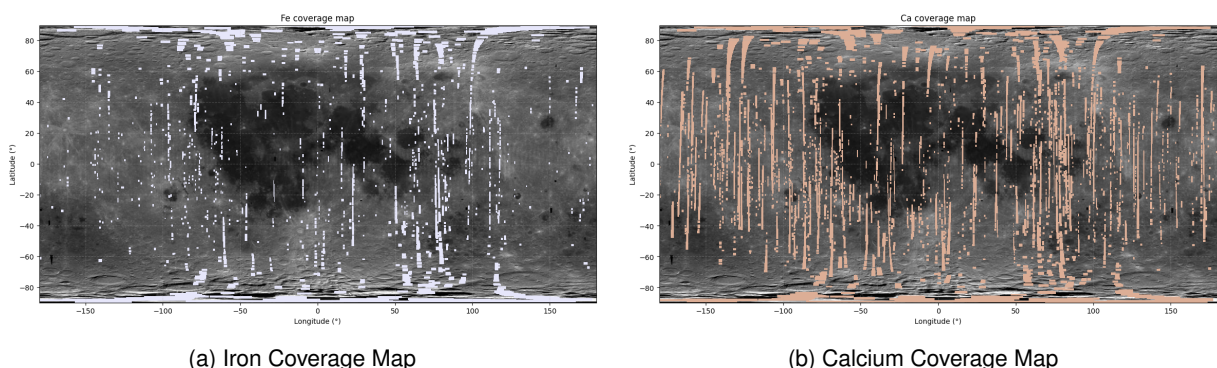


Figure 7: Coverage Maps of Fe and Ca.

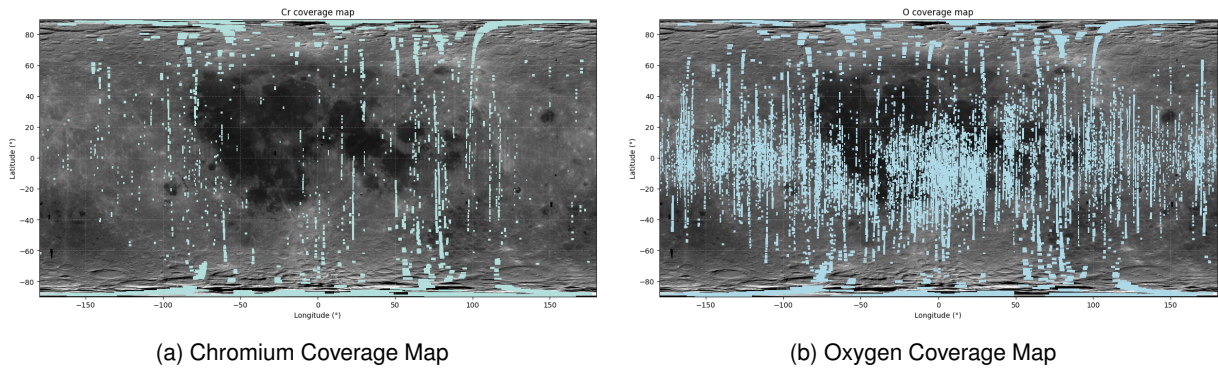


Figure 8: Coverage Maps of Cr and O.

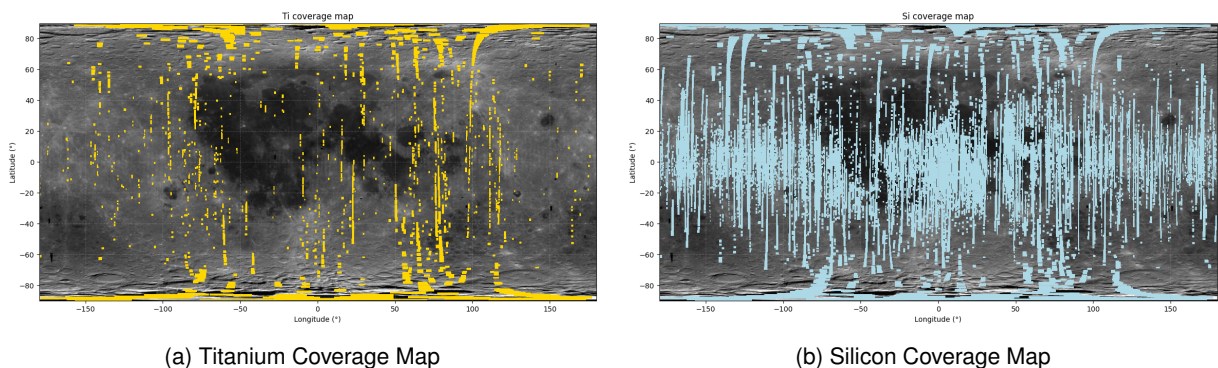


Figure 9: Coverage Maps of Ti and Si

#### 4.B.I. Analysis of Coverage Maps :

The coverage of Mg, Al, and Si is relatively more than that of Ti, Fe, Ca, Cr, and O, which is sparse. This is due to lower detection of those elements following lesser excitation of heavier elements due to higher excitation energy and low detection of O due to less excitation energy.

#### 4.C. Achieve Subpixel Resolution

On increasing the resolution due to consideration of overlapping tracks , the difference in ratios are gradual across consecutive tracks whereas when plotted with a resolution of  $12.5\text{km} \times 12.5\text{km}$ , they are overlapped on each other.

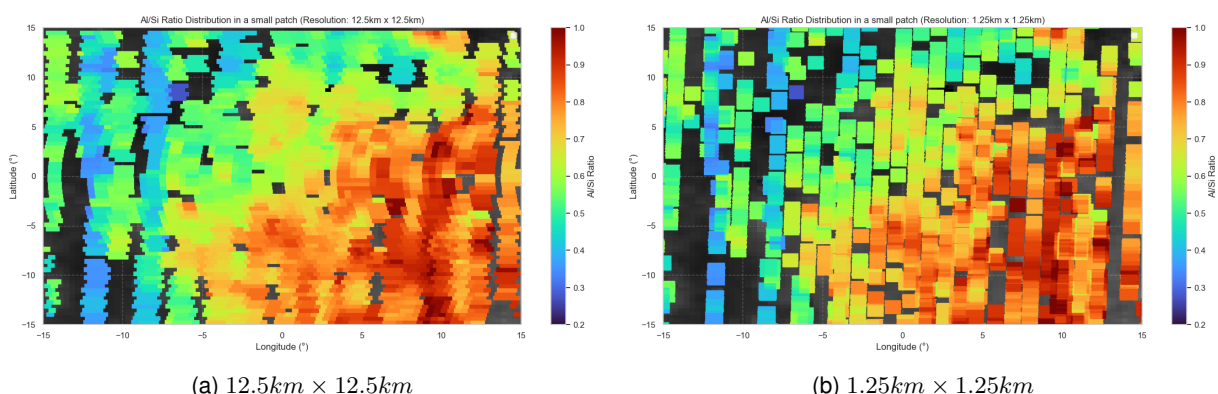


Figure 10: Comparison of resolution between  $12.5\text{km} \times 12.5\text{km}$  and  $1.25\text{km} \times 1.25\text{km}$

#### 4.D. Elemental ratio maps

We can distinguish the elemental ratio variation in different regions of the lunar surface. The ratios vary as we move to Maria and Highlands. Broadly, ratios have different ranges in the Maria region and the Highland region.

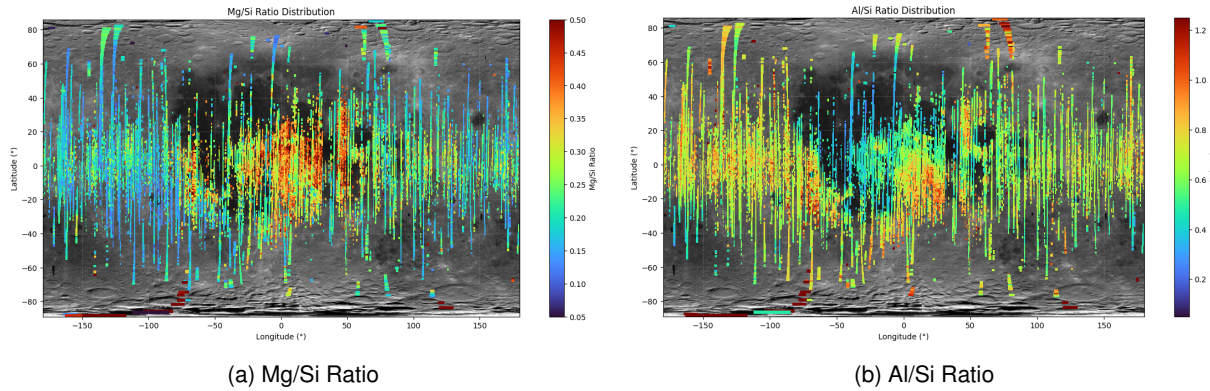


Figure 11: Elemental Ratio Maps: Mg/Si and Al/Si Ratios.

The ratio of Mg/Si is higher in the Maria region, while the ratio of Al/Si is higher in the Highlands region.

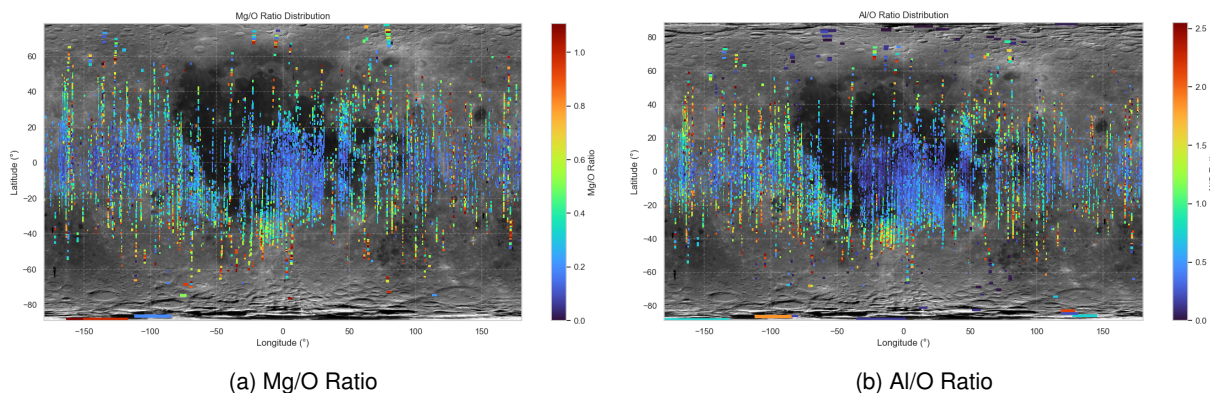


Figure 12: Elemental Ratio Maps: Mg/O and Al/O Ratios

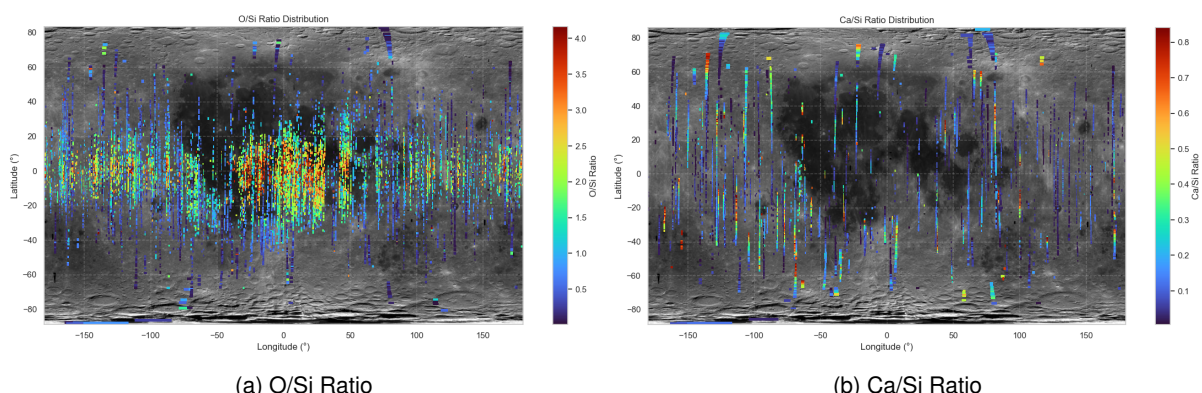


Figure 13: Elemental Ratio Maps: O/Si and Ca/Si Ratio

As calcium (or anorthite molecule) majorly exists as a content of plagioclase, which is evenly distributed on the lunar surface. This is why, here, Ca/Si ratio is almost constant over the lunar surface.

#### 4.D.I. Sub pixel Resolution :

The Al/Si and Mg/Si elemental ratio maps with a resolution of  $3.125\text{km} \times 3.125\text{km}$  are as follows:

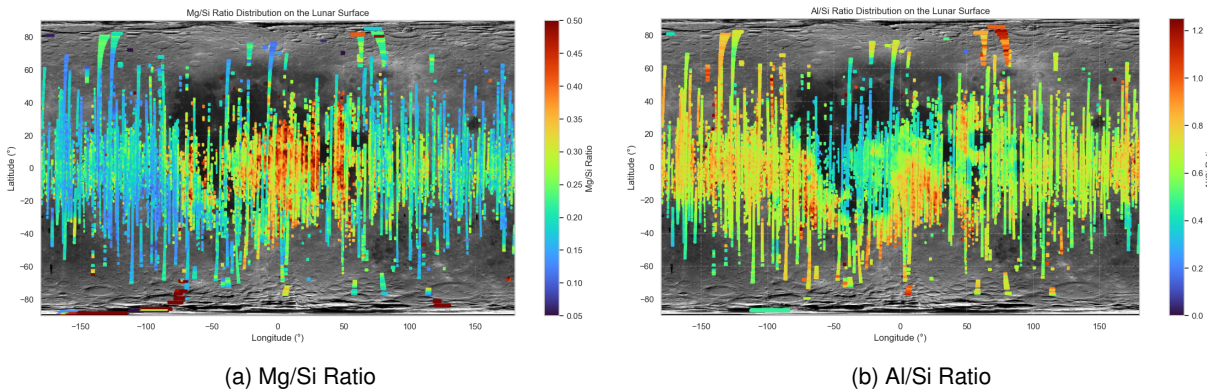


Figure 14: Elemental Ratio Maps at  $3.125\text{ km}$  resolution: Mg/Si and Al/Si Ratios

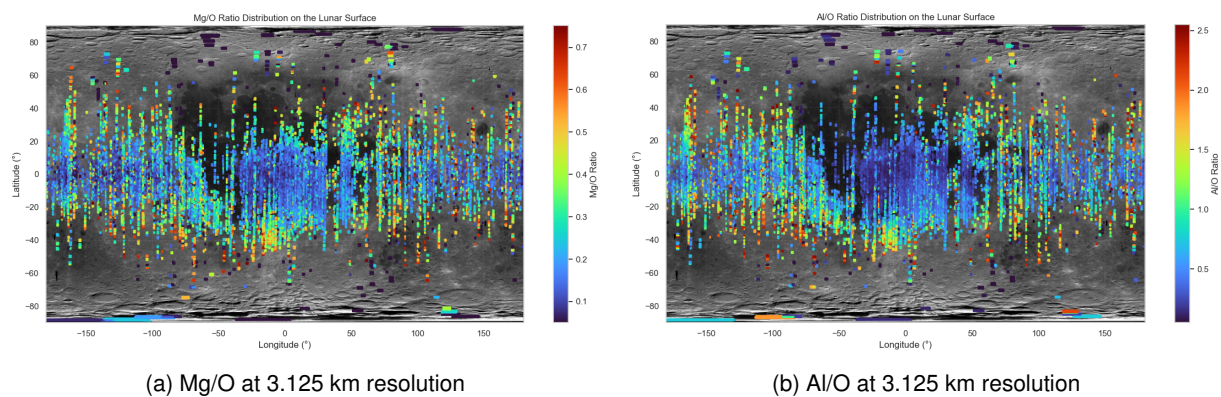


Figure 15: Elemental Ratio Maps at  $3.125\text{ km}$  resolution: Mg/O and Al/O Ratios.

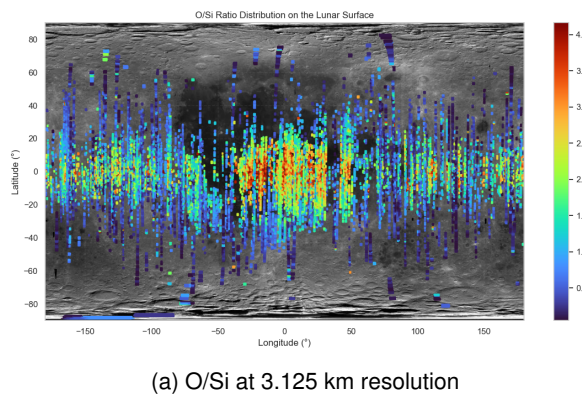


Figure 16: Elemental Ratio Map at  $3.125\text{ km}$  resolution: O/Si Ratios.

#### 4.E. Uncertainty Quantification

Calculating uncertainties is essential when overlapping tracks yield differing measurements for the same position, as these differences may arise from instrumental variations, surface or geophysical inconsistencies, or data processing methods. Uncertainties, such as the SEM, help identify reliable regions with consistent data and highlight areas where variability or errors may exist. This ensures accurate mapping and provides a

measure of confidence for scientific interpretations. In regions with only one observation, uncertainties cannot be calculated, highlighting the need for multiple measurements to ensure robustness. Overall, uncertainties improve map accuracy, guide the interpretation of overlapping tracks, and ensure the reliability of conclusions drawn from the data.

The ratios are calculated for valid entries, and latitude and longitude boundaries for each data point are used to assign the values to spatial grid cells, with grid sizes corresponding to approximately 6.25 km. Each grid cell aggregates these values, calculating the mean and the percentage standard error of the mean (SEM)(%) for the ratios. The gridded data is then visualized on a lunar map, with SEM values represented as color-coded rectangles to highlight areas with greater variability. A box plot of the SEM values is also created to summarize the distribution of uncertainties across the Moon's surface. The processed data and grid statistics are saved as CSV files for further analysis.

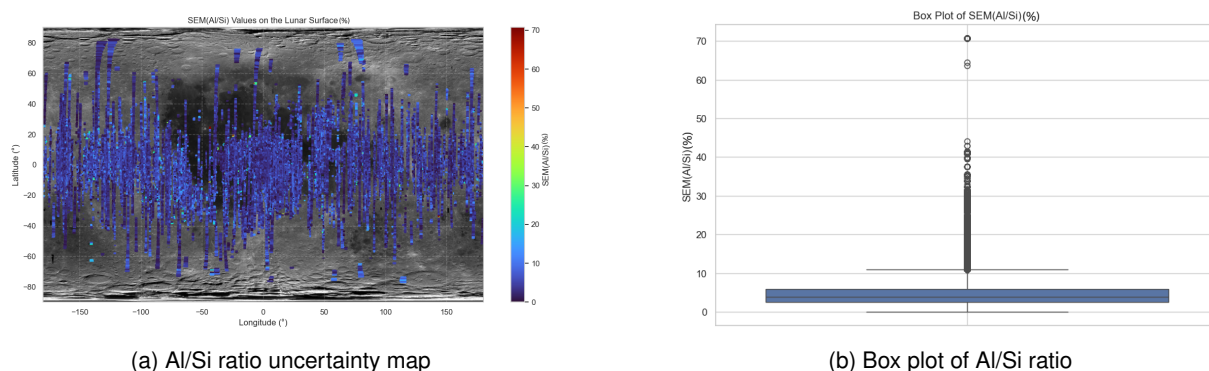


Figure 17: Comparison of Al/Si ratio uncertainty map and box plot.

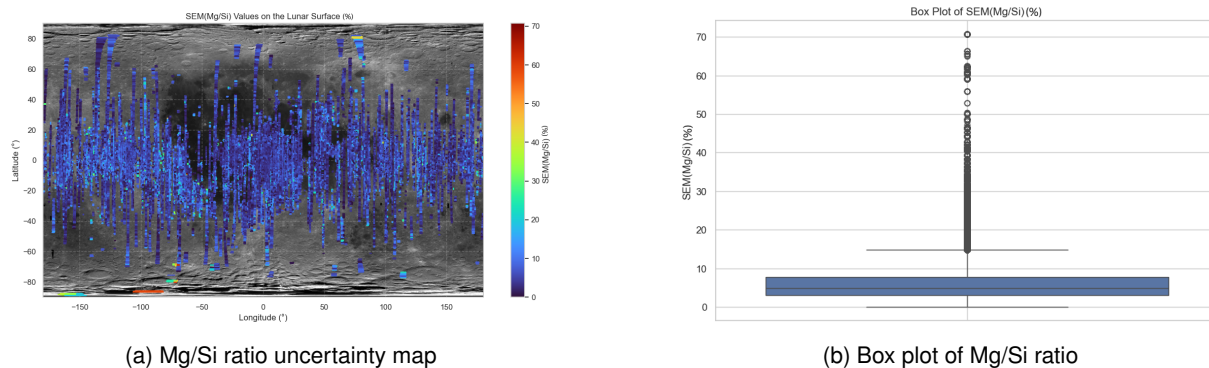


Figure 18: Comparison of Mg/Si ratio uncertainty map and box plot.

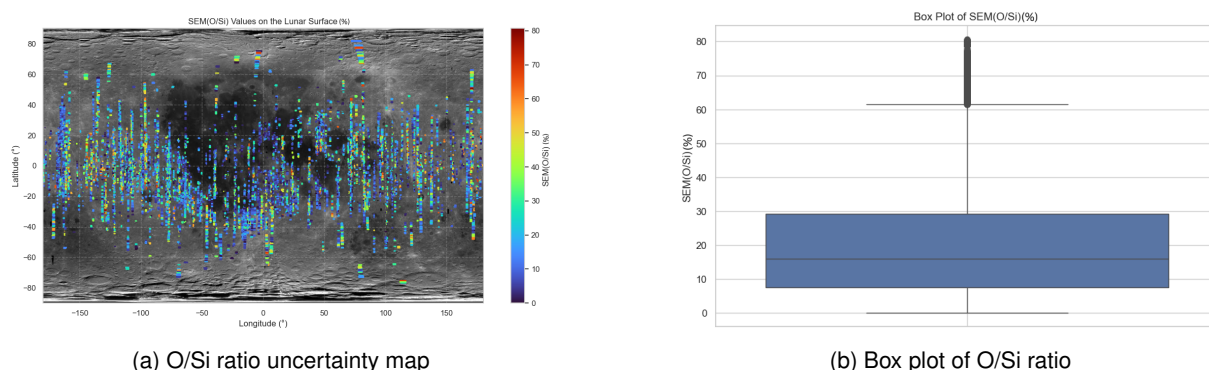
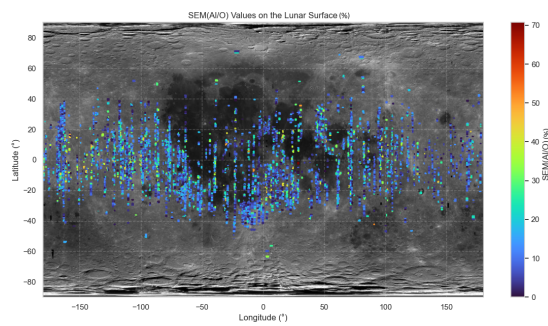
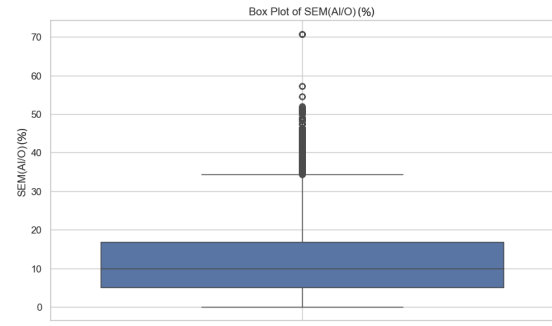


Figure 19: Comparison of O/Si ratio uncertainty map and box plot.

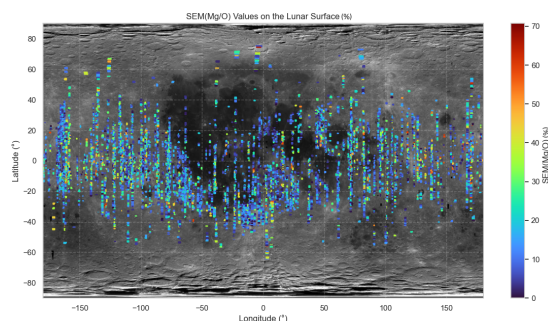


(a) Al/O ratio uncertainty map

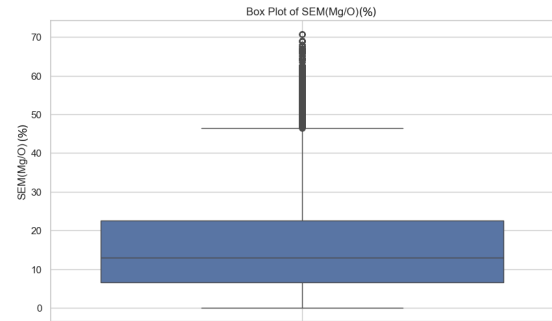


(b) Box plot of Al/O ratio

Figure 20: Comparison of Al/O ratio uncertainty map and box plot.



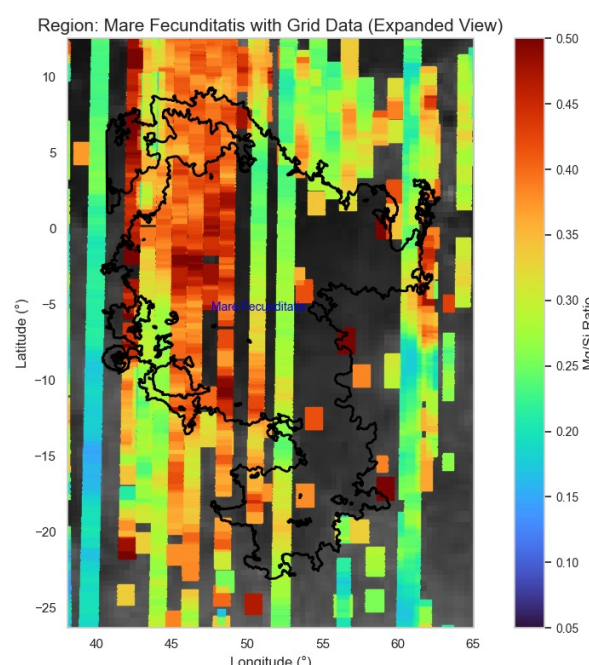
(a) Mg/O ratio uncertainty map



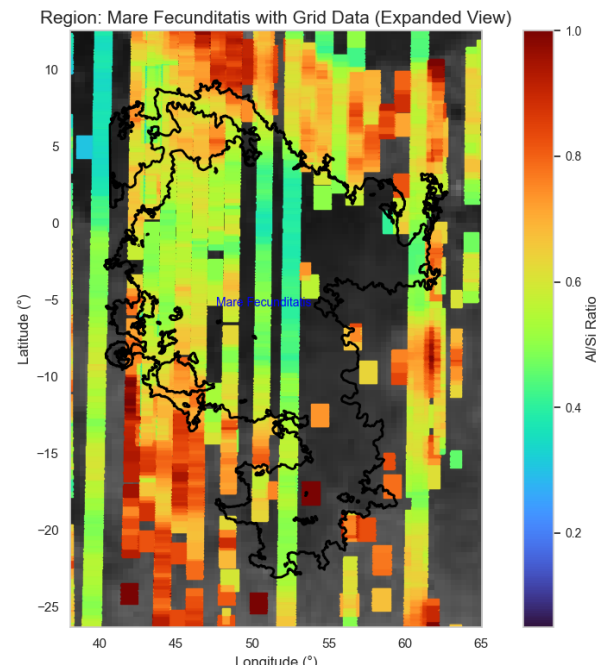
(b) Box plot of Mg/O ratio

Figure 21: Comparison of Mg/O ratio uncertainty map and box plot.

#### 4.F. Visualization at finer scale(1.25km × 1.25km)



(a) Mg/Si Ratio



(b) Al/Si Ratio

Figure 22: Elemental Ratio Maps at Mare Fecunditatis

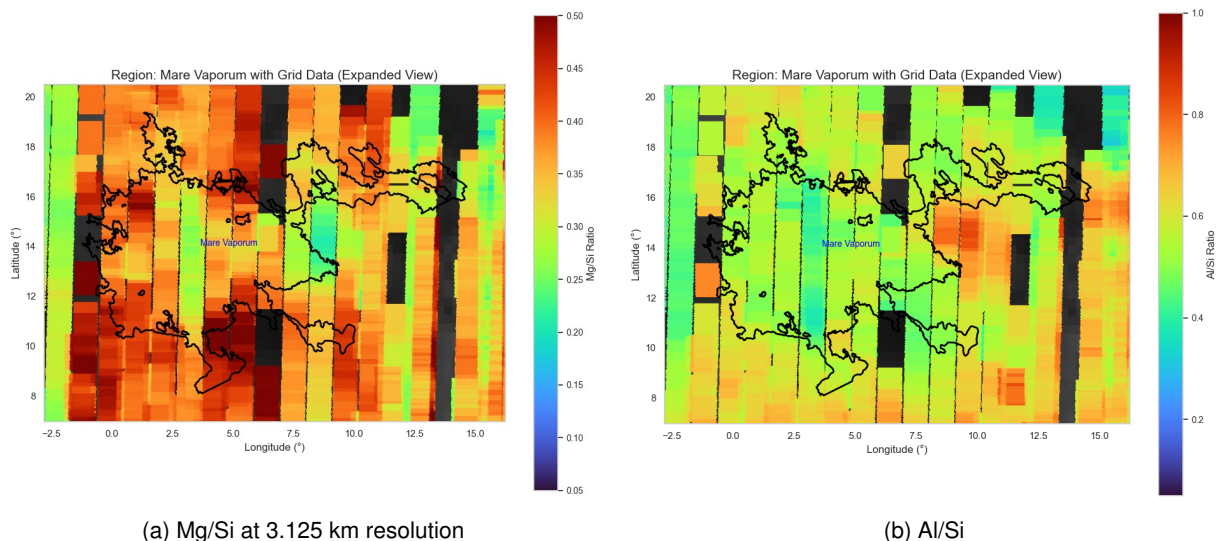


Figure 23: Elemental Ratio Maps at Mare Vaporum

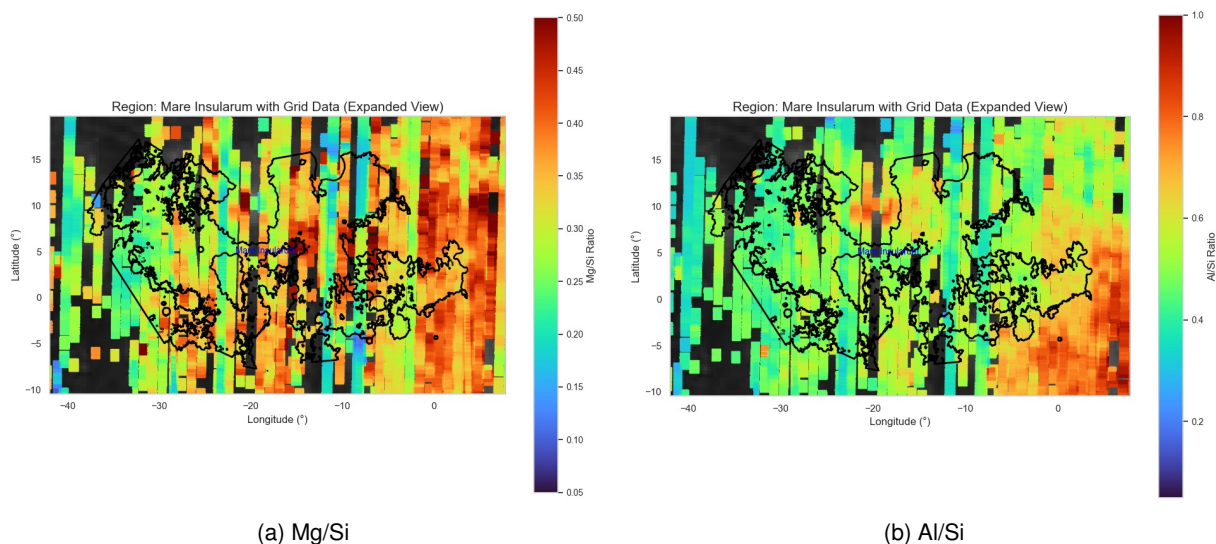


Figure 24: Elemental Ratio Maps at Mare Insularum

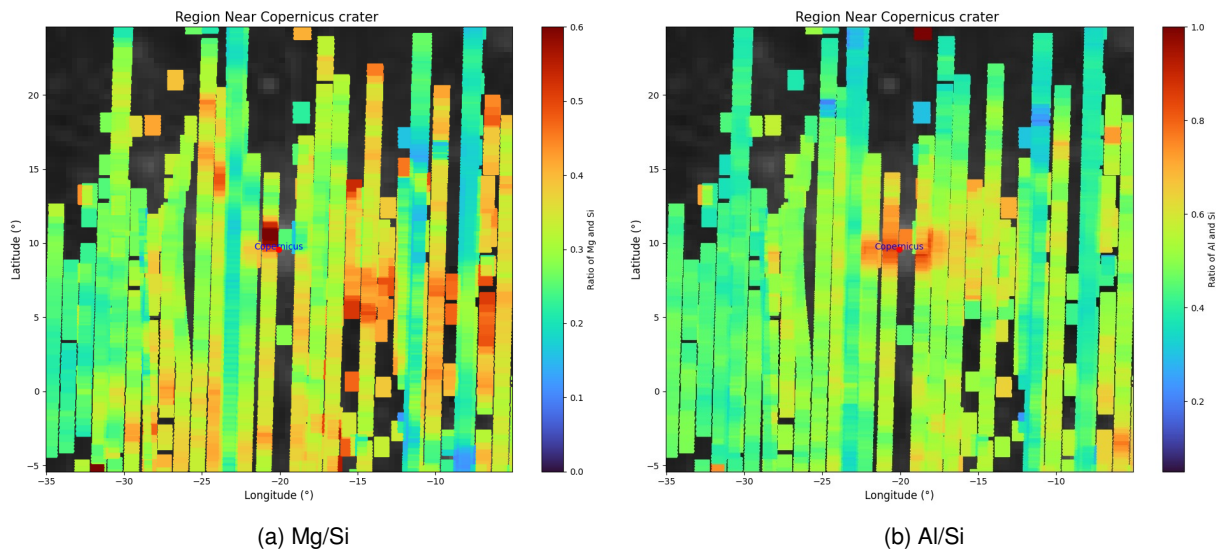
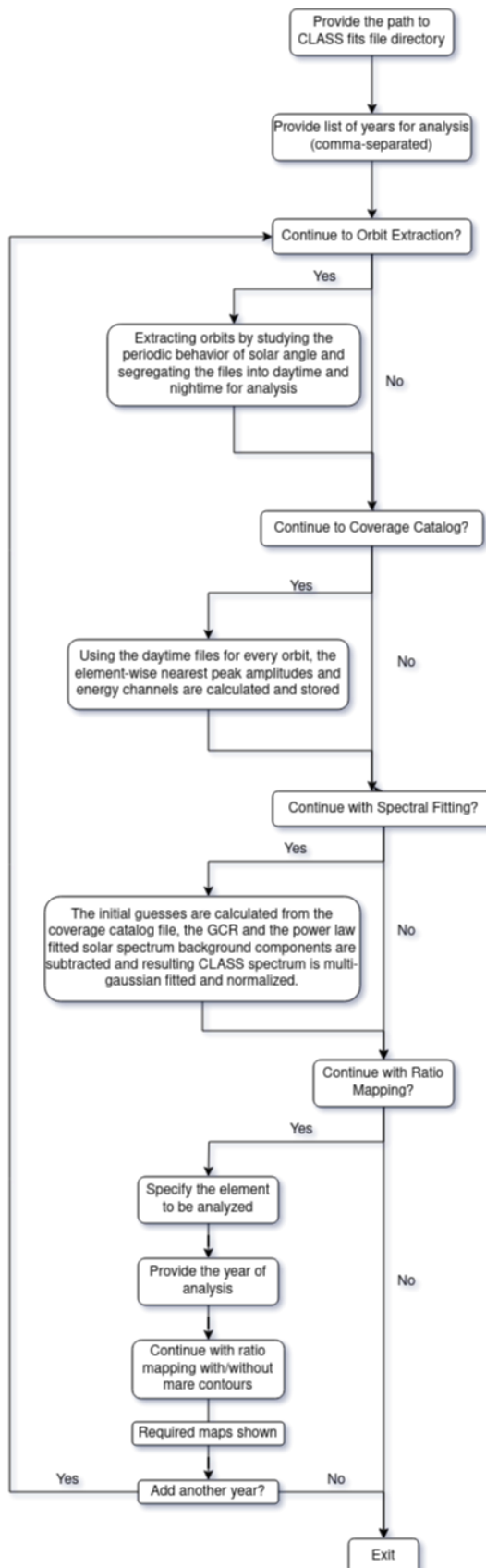


Figure 25: Elemental Ratio Maps at Copernicus crater

## 5. Flow Chart of Procedure



## 6. Challenges and Lessons Learnt

The XRF CLASS data analysis to find elemental ratio composition over the lunar surface consisted few challenges and corresponding learnings to optimize the approach.

- The major challenge in CLASS XRF analysis is the peak detection of elements with higher atomic numbers. CLASS X-ray fluorescence has good sensitivity for lighter elements and provides fairly good results for these elements. Higher excitation energies of heavier elements lead to lesser excitation, and hence, detection of those elements becomes difficult.
- Due to the limited operation of CLASS at night time, we had limited night-time data to calculate night-time background. The most accurate nighttime background would be around the solar phase angle at  $180^\circ$ . Due to limited data of night-time observation, CLASS data above solar phase angle  $91^\circ$  was considered for night time background. However, our empirical analysis showed very little deviation in the nighttime spectrum for nearer solar phase angles post  $90^\circ$  and around solar phase angles  $180^\circ$ . Hence, results for nighttime background post  $91^\circ$  are also fairly accurate.
- Due to limited XSM data for spectral fitting and normalization to remove solar spectrum from XRF received and calculating exact ratios with respect to uniform count spectrum for all channel ranges, total analysis could not be conducted with XSM data. Alternatively, power law fitting provided precise results that were implemented for the whole CLASS analysis.

To tackle these challenges effectively, alternative approaches were developed to optimize the process of finding the elemental ratio, without compromising with correctness of the approach and the accuracy of results.

## 7. Future Scope and Recommendations

For the pre-processing part, the use of the Voigt fitting technique, which is an advanced approach compared to Gaussian fitting, with optimized computational efficiency, could be used for curve fitting in the future. Additionally, with more computational power and more overlapped data, finer and finer resolution maps can be generated.

The lunar south pole has become a focal point for global exploration due to its potential water ice deposits, crucial for human habitation and resource utilization. NASA's Artemis Program, starting with Artemis III in 2026, aims to land astronauts in this region, with SpaceX's Starship delivering crew and supplies for future missions. Similarly, China's Chang'e missions, including Chang'e 7 (2026) and Chang'e 8 (2028), will map water ice, test autonomous technologies, and explore prospects for a research station. ESA's Moonlight initiative (2027–2030) will provide communication and navigation support to complement global South Pole missions. Additionally, the Commercial Lunar Payload Services (CLPS) program will deploy robotic landers and rovers (2024–2028) to study volatiles and advance resource utilization technologies, paving the way for sustainable lunar exploration. From our data, we have identified several areas of significance on the lunar surface that warrant further research and exploration. These regions could provide valuable insights into resource distribution, geological processes, and the potential for supporting future lunar missions.

## 8. References

1. CLASS Manual
2. XSM Manual
3. [2306.13355] Richardson-Lucy deconvolution with a spatially Variant point-spread function of Chandra: Supernova Remnant Cassiopeia A as an Example
4. Deconvolution in X-ray photoelectron spectroscopy - ScienceDirect
5. Experimental methods in chemical engineering: X-ray fluorescence—XRF
6. [https://pradan.issdc.gov.in/ch2/protected/downloadFile/class/ch2\\_class\\_pds\\_release\\_38\\_20240927.zip](https://pradan.issdc.gov.in/ch2/protected/downloadFile/class/ch2_class_pds_release_38_20240927.zip)
7. X-ray fluorescence spectrometry - Journal of Analytical Atomic Spectrometry (RSC Publishing)
8. Chandrayaan-2: India's 2nd Lunar Exploration Mission - IJERT
9. Geology, Geochemistry of Moon
10. Lunar Maria
11. Lunar Compositional Analysis
12. Validation of methodology to derive elemental abundances from X-ray observations on Chandrayaan-1
13. Lunar Sourcebook
14. Research on the inversion of elemental abundances from Chang'E-2 X-ray spectrometry data
15. Lunar elemental abundances as derived from Chandrayaan-2 - ScienceDirect
16. Lunar X-ray fluorescence observations by the Chandrayaan-1 X-ray Spectrometer (C1XS): Results from the nearside southern highlands
17. SHAPEFILE-LROC-GLOBAL-MARE